Chinese Chemical Letters 33 (2022) 4587–4594

Contents lists available at ScienceDirect

Chinese Chemical Letters

journal homepage: www.elsevier.com/locate/cclet

Distachydrimanes A–F, phenylspirodrimane dimers and hybrids with cytotoxic activity from the coral-derived fungus *Stachybotrys chartarum*

Shuang Lin[1], Jianzheng Huang[1], Hanxiao Zeng, Qingyi Tong*, Xueke Zhang, Beiye Yang, Ying Ye, Jianping Wang, Zhengxi Hu*, Yonghui Zhang*

Hubei Key Laboratory of Natural Medicinal Chemistry and Resource Evaluation, School of Pharmacy, Tongji Medical College, Huazhong University of Science and Technology, Wuhan 430030, China

ARTICLE INFO

Article history:
Received 1 December 2021
Revised 14 March 2022
Accepted 15 March 2022
Available online 17 March 2022

Keywords:
Stachybotrys chartarum
Distachydrimanes A–F
Structure elucidation
Cytotoxic activity
Mechanism of action

ABSTRACT

By integrating one strain-many compounds (OSMAC) and LC–MS-based molecular networking strategies, distachydrimanes A–F (**1–6**), six novel phenylspirodrimane dimers and hybrids representing two types of unprecedented terpenoid-polyketide hybrid skeletons, were isolated from the modified fermented rice substrate of a coral-derived fungus *Stachybotrys chartarum*. All the structures incorporating their absolute configurations were elucidated based on comprehensive spectroscopic analyses, mainly including HRESIMS and NMR data, single-crystal X-ray diffraction (Cu Kα), and comparison of the experimental electronic circular dichroism (ECD) data. Architecturally, compounds **1–6** represent an unprecedented class of dimeric phenylspirodrimanes with an unexpected C-18–C-23′ linkage, of which compounds **1–3** also feature an unexpected 5-methyl-1,3-benzenediol moiety *via* a carbon-carbon linkage. The bioactivity assay demonstrated that compounds **1**, **5** and **6** induced cell proliferation inhibition, G0/G1 cell cycle arrest, senescence and mitochondrial-mediated apoptosis in L1210 cells, highlighting their potentials as a new category of anticancer agents.

Cancer poses the greatest incidence and mortality rate worldwide. It was caused by an abnormal cell growth with the ability to invade and spread throughout the organism [1], accounting for an estimated 10 million deaths in 2020 [2]. It is estimated that over the next 20 years, cancer cases are predicted to increase by 60% globally and by up to 81% in low- and middle-income countries [3]. More than that, the current clinical cancer treatments are still faced with recurrence due to the residual cancer cells and minute lesions in surgery, chemotherapy and other treatments [4]. Therefore, there is an urgent need to develop novel drugs for cancer therapy.

Natural products (NPs), isolated from plants, microbes, and even animals, are an immense reservoir of bioactive molecules that play an irreplaceable role in the discovery and development of innovative drugs [5–7]. NPs are thought to have ushered a new golden age since the 2015 Nobel Prize in Physiology or Medicine was awarded to avermectin and artemisinin [8]. Drugs developed from NPs have been confirmed to possess many beneficial pharmacological effects and are widely used to treat various human diseases [9,10], for cancer therapy, such as taxol [11] and doxorubicin [12] are successful precedents.

In recent years, our research team has performed several studies towards chemically novel and bioactive secondary metabolites from fungi inhabiting unique environments [13–18], and a coral-derived fungus *Stachybotrys chartarum* came into our sight. Previously, we have isolated and identified six new dolabellanes and atranones from the title fungus [19]. To tap into the fungus-stored biosynthetic potentials, we adopted the OSMAC strategy by adding 0.1% $Fe_2(SO_4)_3$ and 3% sea salt into the normal rice medium and employed LC–MS/MS–GNPS (Global Natural Product Social Molecular Networking) data to analyze the metabolites. By screening against GNPS spectral database (Fig. 1), four nodes (parent ions at *m*/*z* 429.218, 471.240, 387.217 and 371.139) were identified as stachybotrysin C [20], stachybotrysin H [21], stachybotrylactone [22], and mer-NF5003E [23], respectively, which have been isolated and characterized from the *Stachybotrys* species as potential leads for anticancer, antivirus, anti-inflammatory, and avian myeloblastosis virus protease inhibitor drugs. These analytical data suggested the presence of more bioactive phenylspirodrimane congeners in the metabolites of fungus *S. chartarum*, which stimulated us to ulteriorly investigate this fungus by a large-scale culture [24],

* Corresponding authors.
E-mail addresses: qytong@hust.edu.cn (Q. Tong), hzx616@126.com (Z. Hu), zhangyh@mails.tjmu.edu.cn, zhangyonghui5@sina.com (Y. Zhang).
[1] These authors contributed equally to this work.

https://doi.org/10.1016/j.cclet.2022.03.064
1001-8417/

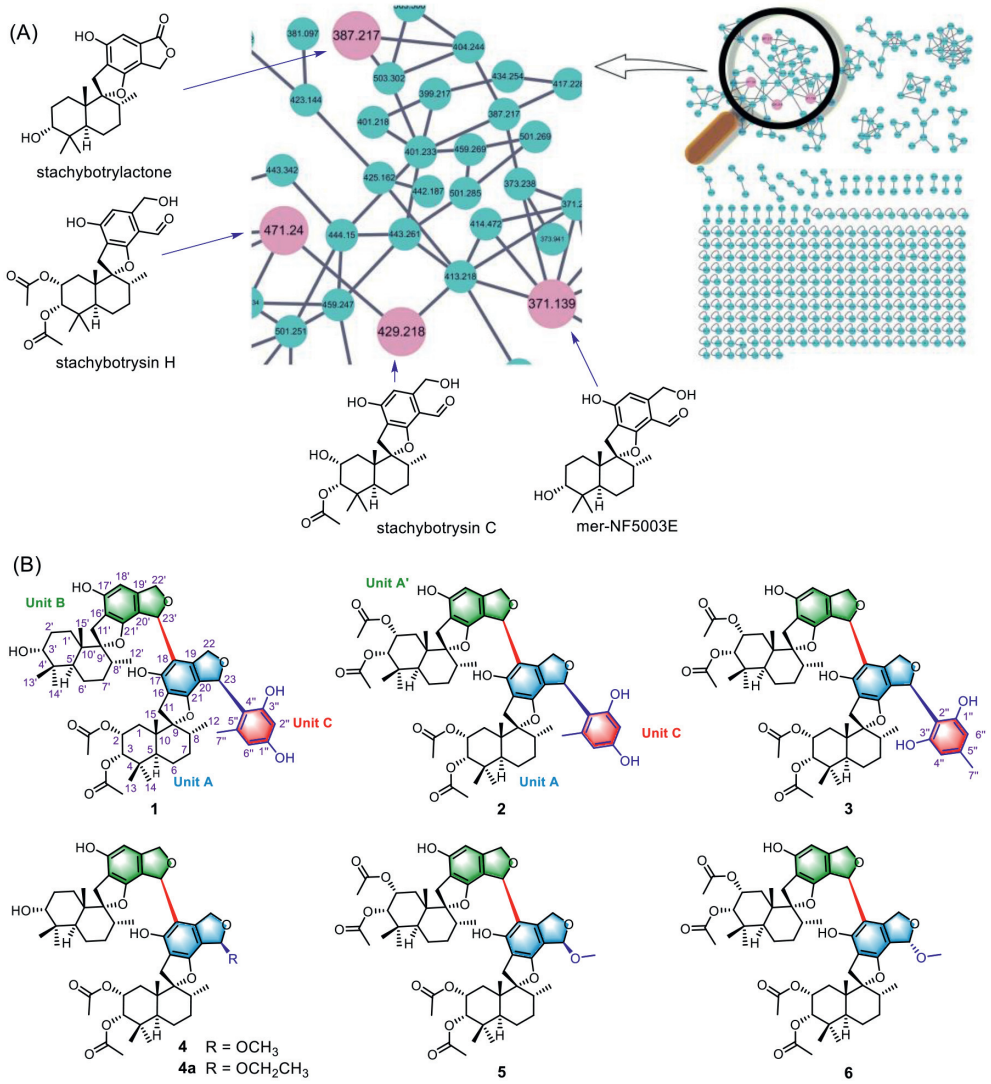

Fig. 1. (A) LC–MS-based molecular networking of an EtOAc extract of fungus *S. chartarum*. (B) Chemical structures of compounds **1**–**6**.

facilitating the isolation and characterization of six novel phenylspirodrimane dimers and hybrids, namely distachydrimanes A–F (**1–6**). Structurally, compounds **1–6** represent a series of skeletally unprecedented dimeric phenylspirodrimanes *via* an unexpected C-18–C-23′ linkage, of which compounds **1–3** are uniquely defined by an unexpected 5-methyl-1,3-benzenediol moiety *via* a carbon-carbon linkage. Additionally, all six compounds showed certain cytotoxic activity, and notably compounds **5** and **6** showed significant cytotoxic activity against all cancer cell lines (< 10 μmol/L). Herein, the detailed isolation, structure elucidation, cytotoxic activity and the preliminary mechanism of these compounds are described.

Strain *S. chartarum* was cultured on potato dextrose agar (PDA) plates at 28 °C for 7 days to prepare the seed cultures. Agar plugs were cut into small pieces (approximately $0.2 \times 0.2 \times 0.2$ cm^3) and inoculated into 400 Erlenmeyer flasks (1 L), previously sterilized by autoclaving, each containing 250 g of rice and 250 mL of distilled water (adding 0.1% $Fe_2(SO_4)_3$ and 3% sea salt). All flasks were incubated at 28 °C for 30 days. The growth of fungus was stopped by adding 250 mL of 95% EtOH to each flask, and the solvent was decanted and removed under reduced pressure. The rice cultures were soaked with the recycled EtOH five times until the solvent extract was nearly colorless at room temperature. The concentrated extract was suspended in water (3 L) and extracted with EtOAc (1:1, v/v) three times to obtain a total residue of 400 g.

The EtOAc residue was fractionated on RP-C_{18} silica gel CC eluted with MeOH–H_2O (20%, 40%, 50%, 60%, 80%, and 100%) to give four main fractions (A–D). Fraction B (MeOH–H_2O, 60:40, v/v) was loaded onto Sephadex LH-20 (CH_2Cl_2–MeOH, 1:1, v/v) and silica gel CC eluted with petroleum ether–ethyl acetate (5:1, 2:1, 1:1, and 0:1, v/v) to give seven main fractions (B1–B7) by TLC analysis. Fraction B2 was subjected to RP-C_{18} column chromatography eluted with a step gradient of MeOH–H_2O (from 20:80 to 80:20, v/v) to yield seven fractions (B2-1–B2-7) in total. Fraction B2-4 was separated by semi-preparative HPLC (MeCN–H_2O, 89:11, v/v; 2.0 mL/min) to afford compound **5** (5.2 mg, t_R 30.1 min). Fraction B2-5 was subjected to semi-preparative HPLC (MeOH–H_2O, 88:12, v/v; 2.0 mL/min) to afford compound **4** (4.9 mg, t_R 20.5 min). Fraction B5 was separated into four fractions (B5-1–B5-4) by Sephadex LH-20 eluted with CH_2Cl_2–MeOH (1:1, v/v). Fraction B5-1 was purified *via* semi-preparative HPLC (MeCN–H_2O, 80:20, v/v; 2.0 mL/min) to provide compounds **2** (3.9 mg, t_R 19.5 min) and **3** (2.9 mg, t_R 30.5 min). Fraction B5-2 was consecutively separated by semi-preparative HPLC (MeOH–H_2O, 81:19, v/v; 2.0 mL/min) to provide compound **1** (7.4 mg, t_R 12.0 min). Fraction B6 was applied to Sephadex LH-20 (CH_2Cl_2–MeOH, 1:1, v/v) and silica gel

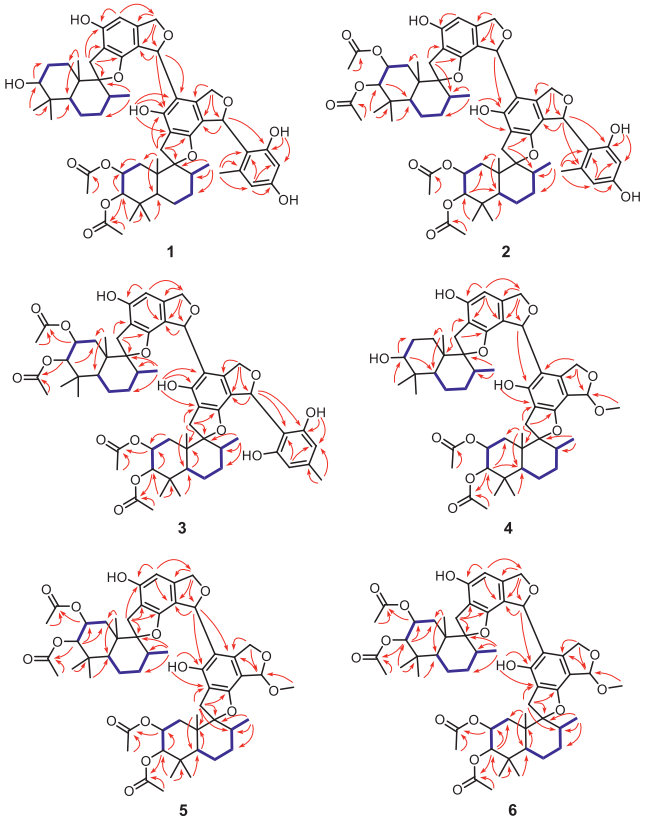

Fig. 2. Selected ^{1}H–^{1}H COSY (blue bold lines) and HMBC (red single arrows) correlations of **1–6**.

CC eluted with petroleum ether–ethyl acetate (5:1, 3:1, 2:1, and 1:1, v/v) to obtain four main fractions (B6-1–B6-4) by TLC analysis. Fraction B6-2 (petroleum ether–ethyl acetate, 3:1, v/v) was purified *via* semi-preparative HPLC (MeCN–H_2O, 92:8, v/v; 2.0 mL/min) to afford compound **6** (5.2 mg, t_R 35.8 min).

Distachydrimane A (**1**) was obtained as a colorless crystal with a molecular formula of $C_{57}H_{72}O_{13}$, as deduced from the HRESIMS data at *m/z* 987.4848 $[M+Na]^+$ (calcd. for 987.4865), corresponding to 22 degrees of unsaturation. The IR spectrum of **1** showed absorption bands for hydroxy (3420 cm^{-1}), ester carbonyl (1744 and 1719 cm^{-1}) and double bond (1627 cm^{-1}) groups. The ^{13}C and DEPT NMR data (Table S2 in Supporting information) revealed 57 carbon resonances, including 11 methyl carbons, 11 methylene carbons (including two oxygenated), nine methine carbons (including five oxygenated), six quaternary carbons (including two oxygenated), 18 aromatic carbons for three phenyl groups, and two ester carbonyl carbons. Combined with the ^{1}H NMR data (Table S1 in Supporting information) of compound **1**, the typical signals including two oxygenated methylenes at δ_H 5.32/5.68 and 4.99/5.09 and eight methyls at δ_H 0.27, 0.22, 0.99, 0.87, 0.92, 1.10, 0.98, and 0.94 for a phenylspirodrimane dimer backbone were observed. Further analysis of 2D NMR data (Fig. 2) validated the presence of two structurally similar phenylspirodrimane monomers, except that two acetyl groups were respectively attached to C-2 and C-3 in unit A and only one hydroxy group was attached to C-3′ in unit B. Moreover, the essential signals were carefully assigned by the HMBC correlations from H-23′ to C-18 and C-20′ (Fig. 2), which established an unexpected C-18–C-23′ linkage between units A and B. Interestingly, an extra 4-substituted-5-methyl-1,3-benzenediol moiety (unit C) was attached to C-23, which could be discerned by the HMBC correlations from H-23 to C-3″/C-5″, from H-6″ to C-1″/C-2″, from OH-3″ to C-2″/C-3″, and from H_3-7″ to C-4″/C-5″/C-6″ (Fig. 2). Therefore, the planar structure of **1** was defined, which represents the first example of dimeric phenylspirodrimane featured by an unexpected C-18–C-23′ linkage (units A and B) and hybrid with an unusual 5-methyl-1,3-benzenediol moiety.

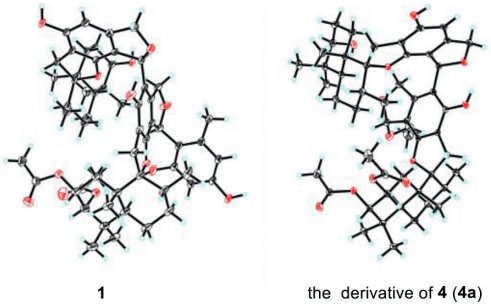

Fig. 3. X-ray ORTEP drawings of compounds **1** and **4a**.

The relative configuration of **1** was determined by analysis of the coupling constant and NOESY data (Fig. S1 in Supporting information). With the fact that H-3 and H-3′ of phenylspirodrimane-type sesquiterpenoids maintained the β-orientation [25], and the small coupling constant between H-2 and H-3 (J = 2.5 Hz) inferred that they were in the *cis*-relationship, therefore H-2, H-3 and H-3′ were all assigned to be β-oriented. The NOESY correlations of H_3-13/H-2/H-3, H-2/H_3-15, H_3-15/H-8, H_3-15/H-11b and H-8/H-11a in unit A, as well as H_3-13′/H-2′β/H-3′, H-2′β/H_3-15′, H_3-15′/H-8′, H_3-15′/H-11′b and H-8′/H-11′a in unit B, indicated that H_3-13/13′, H_3-15/15′, H-8/8′ and CH_2-11/11′ were β-oriented just like H-2 and H-3/3′, whereas the NOESY cross-peaks of H_3-14/H-5 and H_3-14′/H-5′ suggested that H_3-14/14′ and H-5/5′ were on the opposite side with α-orientations. These results were supportive of the common configurations at all corresponding chiral centers as reported phenylspirodrimane dimers [25]. Crucially, the diagnostic NOESY correlations of H_3-14′/H-23 and H-23′/H-22a/H-22b were observed, which implied the α-orientation of H-23/23′.

Regarding the novelty and complexity of **1**, we attempted recrystallization in various two-phase or three-phase solvent systems to address the issue of growing suitable crystals for X-ray diffraction experiment so as to furnish solid evidence for its structure. Fortunately, a high-quality crystal was obtained from CH_2Cl_2–EtOH–H_2O (10:10:1), which was then successfully analyzed by single-crystal X-ray diffraction with Cu Kα radiation (Flack parameter = –0.04(6); Fig. 3). Accordingly, the absolute configuration of **1** was unambiguously determined as 2*R*,3*S*,5*S*,8*R*,9*R*,10*S*,23*S*,3′*R*,5′*S*,8′*R*,9′*R*,10′*S*,23′*S*.

Distachydrimane B (**2**) was isolated as a colorless oil. Its molecular formula was determined as $C_{61}H_{76}O_{16}$ by the HRESIMS analysis (*m/z* 1087.5095 $[M+Na]^+$, calcd for 1087.5026), indicating 24 indices of hydrogen deficiency. The 1D NMR data (Tables S1 and S2) of **2** showed high similarities to those of **1**, implying that **2** was also a phenylspirodrimane dimer. The obvious differences were that a methylene (δ_C 24.3, C-2′) in **1** was replaced by an oxymethine (δ_C 68.2, C-2′) in **2** and two acetyl groups were severally connected to C-2′ and C-3′, suggesting the replacement of unit B in **1** by unit A' in **2**. This assumption was further confirmed by the key ^{1}H–^{1}H COSY correlation of H-2′ (δ_H 5.24)/H-3′ (δ_H 5.03) and HMBC correlations as shown in Fig. 2.

Compound **2** has one more chiral center C-2′ than that of **1**, and the small coupling constant between H-2′ and H-3′ (J = 2.8 Hz) implied that they were also in the *cis*-relationship and assigned as β-oriented (in unit A'). The NOESY cross-peaks of **2** highly resembled those of **1** as shown in Fig. S1, indicating that units A and A' in **2** possessed the same relative configurations as those of **1**. The same biosynthetic pathways and closely similar ECD curves

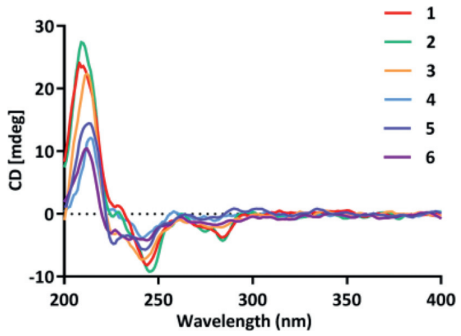

Fig. 4. Experimental ECD spectra of **1–6**.

(Fig. 4) of **1** and **2** suggested the absolute configuration of **2** to be 2/2′*R*,3/3′*S*,5/5′*S*,8/8′*R*,9/9′*R*,10/10′*S*,23/23′*S*.

Distachydrimane C (**3**) was deduced to have a molecular formula of $C_{61}H_{76}O_{16}$, according to the HRESIMS data (*m/z* 1087.5001 $[M+Na]^+$, calcd. for 1087.5026), which was the same as that of **2**. Comprehensive analysis of the NMR data (Tables S1 and S2) of **3** and **2** suggested that both compounds were structural congeners, except for the part of unit C. Two pairs of carbons with the equal chemical shifts (δ_C 155.1, C-1′′/3′′; δ_C 112.0, C-4′′/6′′) were observed on the benzene ring in unit C, suggesting the replacement of a 4-substituted-5-methyl-1,3-benzenediol moiety in **2** by a 2-substituted-5-methyl-1,3-benzenediol moiety in **3**, which can be confirmed by the detailed ^1H–^1H COSY and HMBC correlations as shown in Fig. 2. The similar NOE data and ECD curves (Fig. 4) of **2** and **3** allowed an explicit assignment of the absolute configuration of **3** as 2/2′*R*,3/3′*S*,5/5′*S*,8/8′*R*,9/9′*R*,10/10′*S*,23R/23′*S*.

Distachydrimane D (**4**) had the molecular formula $C_{51}H_{68}O_{12}$ with 18 indices of unsaturation, which was determined by the HRESIMS data (*m/z* 895.4606 $[M+Na]^+$, calcd. for 895.4603). Analysis of the NMR data (Tables S1 and S2) of **4** suggested that it was also a phenylspirodrimane dimer and two phenylspirodrimane monomers of **4** were the same as those of **1**, which could be further demonstrated by the HMBC and ^1H–^1H COSY correlations (Fig. 2). The only imparity was that a methoxy group (δ_C 51.0) linked to C-23 in **4** replaced a 4-substituted-5-methyl-1,3-benzenediol moiety at the same position in **1**, which was confirmed by the key HMBC correlation from OCH_3-23 (δ_H 3.23) to C-23 (δ_C 105.5). Similar NOESY data and ECD curves (Fig. 4) of **1** and **4** suggested that both compounds shared the identical absolute configuration. To further verify this conclusion by a more reliable method, the recrystallization experiment was attempted with various two-phase or three-phase solvent systems under atmospheric conditions. Luckily, the mixed CH_2Cl_2–EtOH–H_2O (10:10:1, v/v/v) solutions of **4** afforded crystals suitable for X-ray crystallography, and they were explicitly identified as ethoxylate **4a**, which could also be supported by the evidence that a C-23 methoxy group disappeared and an ethoxy group (δ_H 3.72, 2H, q, $J=7.1$ Hz; δ_H 1.23, 3H, dd, $J=7.1$, 1.8 Hz) existed in **4a** (Fig. S56 in Supporting information). The crystallography data [Flack parameter = –0.10(5)] demonstrated the absolute stereochemistry of **4a** to be 2*R*,3*S*,5*S*,8*R*,9*R*,10*S*,23*R*,3′*R*,5′*S*,8′*R*,9′*R*,10′*S*,23′*S* (Fig. 3), which was identical to that of **4**. Accordingly, the absolute structure of **4** was defined.

Distachydrimane E (**5**) was assigned to a molecular formula of $C_{55}H_{72}O_{15}$ by the HRESIMS analysis at *m/z* 995.4735 $[M+Na]^+$ (calcd. for 995.4763). The 1D NMR data (Tables S1 and S2) of **5** showed a close structural resemblance to those of **2**, defining that a 4-substituted-5-methyl-1,3-benzenediol moiety in **2** was replaced by a methoxy group (δ_C 51.3) linked to C-23 in **5**, which was supported by the key HMBC correlation from the proton of methoxy group to C-23 (Fig. 2). The same NOESY correlations of **5** and **2** could be discernible and their ECD spectra showed similar Cotton effects (Fig. 4), which suggested the absolute configuration of **5** could also be assigned as 2/2′*R*,3/3′*S*,5/5′*S*,8/8′*R*,9/9′*R*,10/10′*S*,23R/23′*S*.

Distachydrimane F (**6**) was deduced as a C-23 epimer of **5** from their identical HRESIMS ion peaks and awfully similar 1D NMR data (Tables S1 and S2), except that the discernible signals C-23 (δ_C 107.5) and OCH_3-23 (δ_C 56.4) of **6** were distinguished from C-23 (δ_C 105.6) and OCH_3-23 (δ_C 51.3) of **5**. Crucially, the diagnostic NOESY correlation of the methoxy proton (δ_H 3.51) to H_3-14′ further verified the *S*-configuration of C-23 in **6** (Fig. S1). The absolute configurations of all other chiral centers were deduced to be the same as those of **5** (2*R*,3*S*,5*S*,8*R*,9*R*,10*S*,2′*R*,3′*S*,5′*S*,8′*R*,9′*R*,10′*S*,23′*S*) by comparing their identical NOESY correlations and ECD curves (Fig. 4).

Distachydrimanes A–F (**1–6**) represent two special classes of dimeric phenylspirodrimanes with unprecedented carbon skeletons. Their plausible biosynthetic pathways are proposed as follows (Scheme 1). A series of phenylspirodrimane monomers including stachybotrysin C, stachybotrysin H, and mer-NF5003E, are derived from orsellinic acid and farnesyl diphosphate (FPP) through key prenylation, cyclization, and redox reactions [26]. Further hydroxylation, methylation and dehydration reactions afford intermediates **i** and **ii**, which undergo a further Friedel-crafts reaction *via* an unexpected C-18–C-23′ bond to generate an intermediate **iii**. Selective acetylation of rings A/A' of **iii** could create compounds **4–6**. On the other hand, after the removal of methoxy, **iii** undergoes a key Friedel-crafts reaction with a small molecule orcinol *via* a carbon-carbon linkage, and further oxidation and acetylation reactions to produce compounds **1–3**.

The bioactivity of compounds **1–6** against seven cancer cell lines was initially assessed by a CCK-8 kit, and etoposide (VP16) was used as the positive control. Compounds **5** and **6** showed significant anti-proliferation effect against all cancer cell lines, with IC_{50} values ranging from 2.66 μmol/L to 8.14 μmol/L, and compounds **1**, **3** and **4** also showed remarkable anti-proliferation effect against most of these cancer cell lines, especially to L1210 (Table S3 in Supporting information; Figs. 5A–C). Regarding the yield and novelty of these chemical structures, compounds **1**, **5** and **6** were chosen to further explore the anti-proliferation effect and mechanism of this kind of compounds. We first detected the signaling of S6 ribosomal protein, which is a marker of cell proliferation, mitogenic stimulation and overexpressed in various cancers [27]. Compounds **1**, **5** and **6** treatments showed no effect on S6, but significantly inhibited its phosphorylated form after 24 h, and even a complete inhibition was found after compound **1** treatment for 48 h (Fig. 5D). These results demonstrated that the proliferation inhibition effects of compounds **1**, **5** and **6** were associated with the down-regulation of S6 phosphorylation. Moreover, cell morphological changes were very obvious. Microscopic imaging showed that, after compounds **1**, **5** and **6** treatments, some cells shrank and became dense, and some cells featured cytoplasmic swelling and plasma membrane bubbles featured classic apoptotic bodies (Fig. 5E), suggesting that these compounds probably induced apoptosis.

Thus, we performed the apoptosis assays. The induction of apoptosis was first evaluated by DAPI nuclear staining, and the results indicated that compounds **1**, **5** and **6** treatments induced significant stronger blue stain, which labeled the internucleosome fragmentation of genomic DNA during apoptosis (Fig. 6A). Apoptosis was further detected and quantified by Annexin V-FITC/PI staining kit and flow cytometer. Compounds **1**, **5** and **6** (10, 10 and 5 μmol/L, respectively), treated for 48 h caused 78.9%, 82.6% and 48.6% apoptosis in L1210 cells, respectively (Fig. 6B). To further explore the mechanism of apoptosis induction effect of compounds **1**, **5** and **6**, the mitochondrial membrane potential (MMP) of L1210

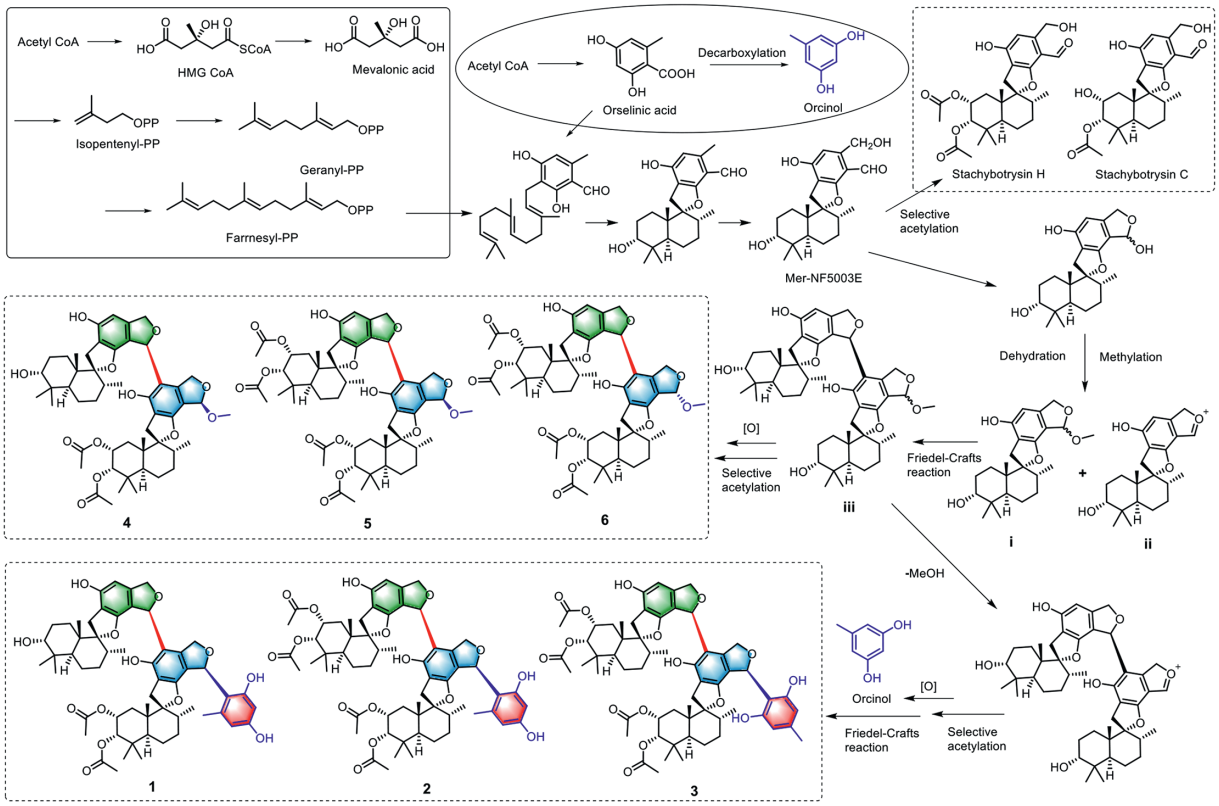

Scheme 1. Plausible biosynthetic pathways for compounds **1–6**.

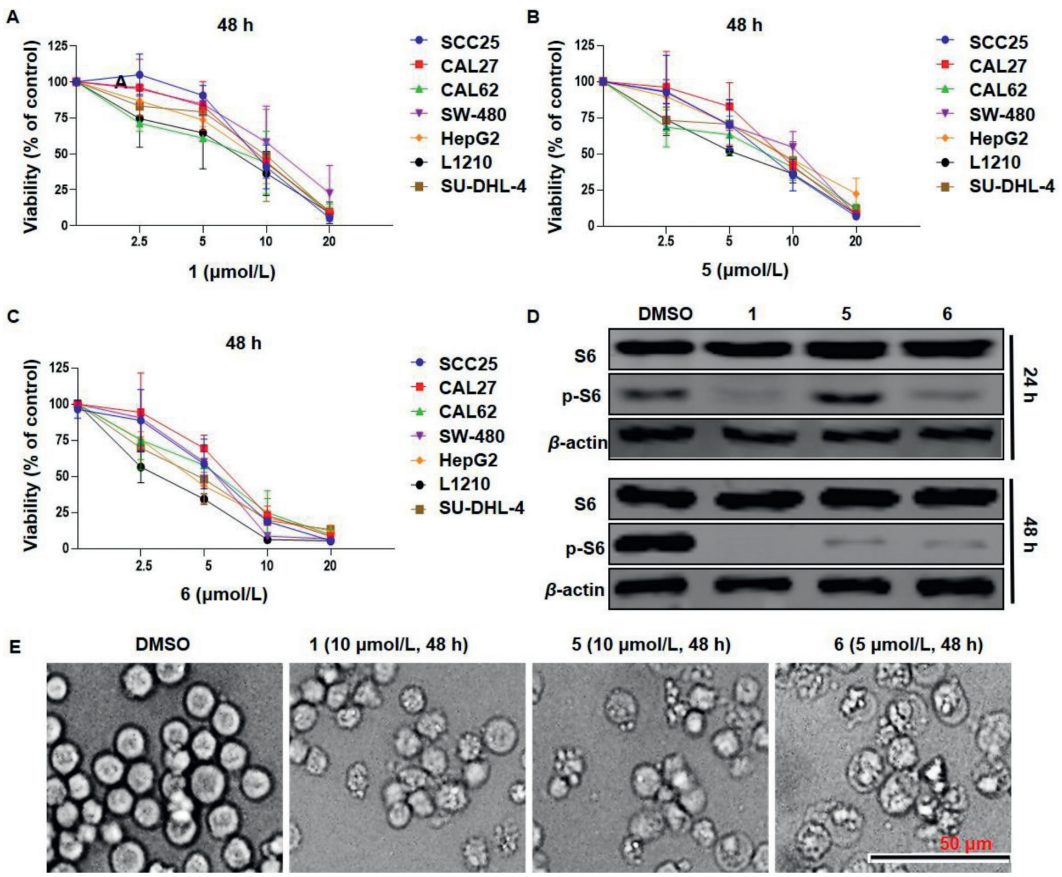

Fig. 5. Compounds **1**, **5** and **6** inhibit cell proliferation and cause morphological changes in L1210 cells. (A–C) Dose-response viability curve of L1210 and other cancer cells after 48 h treatment. Values were mean ± SD of three independent experiments. (D) After treated with compounds **1** (10 μmol/L), **5** (10 μmol/L) and **6** (5 μmol/L) for 24 h and 48 h, the expression of S6 and phospho-S6 (Ser235/236) were evaluated by western blot. β-Actin was used as a loading control. (E) Morphological changes in L1210 cells.

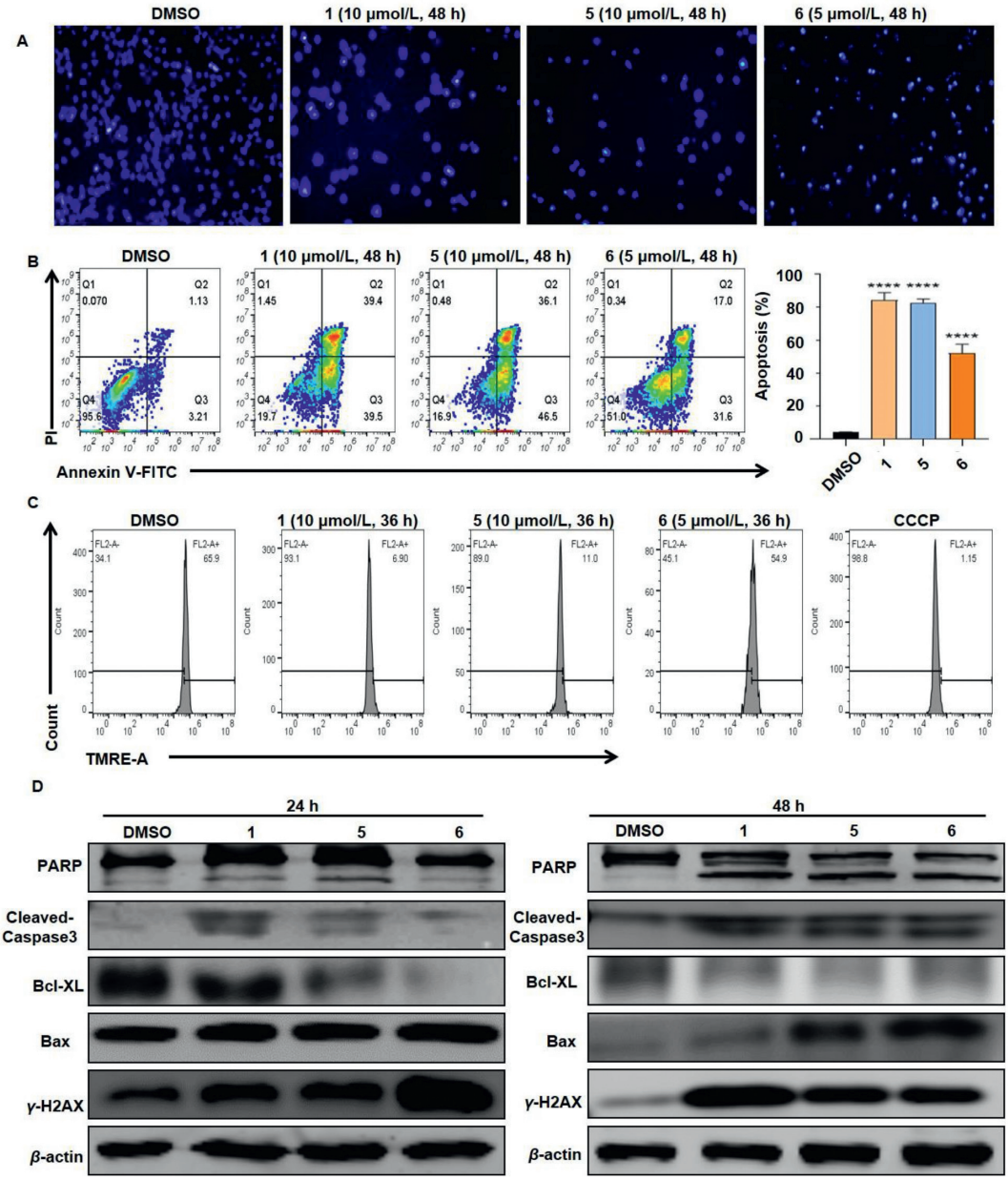

Fig. 6. Compounds **1**, **5** and **6** induce mitochondria-mediated apoptosis in L1210 cells. After treated with compounds **1** (10 μmol/L), **5** (10 μmol/L) and **6** (5 μmol/L), cell apoptosis was evaluated by DAPI staining (A) and Annexin V-FITC/PI staining kit followed by flow cytometer. Columns, means of three different experiments; bars, SD, $^{***}P < 0.001$ against DMSO (< 0.1%) group (B). (C) Mitochondrial membrane potential of the cells was analysed with a TMRE staining kit after 36 h. (D) Western blot analysis of the apoptosis related proteins after 24 h and 48 h treatment. β-Actin was used as a loading control.

cells was evaluated. As shown in Fig. 6C, compounds **1**, **5** and **6** (especially **1** and **5**) treatments decreased MMP of L1210 cells, suggesting that mitochondria may be involved in their apoptotic induction effect. In order to confirm this, proteins of Bcl-2 family as well as the cleaved-caspase 3, PARP were detected. As shown in Fig. 6D, treatments of compounds **1**, **5** and **6** altered the expression levels of PARP, cleaved-caspase 3, Bcl-XL and Bax. The DNA damage marker γ-H2AX also sharply increased after treated with compounds **1**, **5** and **6**. Taken together, these data suggested that compounds **1**, **5** and **6** induced mitochondrial-mediated apoptosis in L1210 cells.

Cell proliferation, DNA damage and apoptosis are closely related to the cell cycle. Our results showed that compounds **1**, **5** and **6** treated for 24 h induced G0/G1 arrest in L1210 cells (Figs. 7A and B). As arrest in the G0/G1 phase of cell cycle has been considered as a marker of senescent cells [28], we next detected cellular senescence with SA-β-gal staining in L1210 cells treated with compounds **1**, **5** and **6** in low concentrations, and all of them induced cellular senescence (Fig. 7C). At the molecular level, treatments of **1**, **5** and **6** up-regulated the expression levels of checkpoint proteins involved in the regulation of the G1/S transition including cyclin D2, CDK2 and CDK6, and also up-regulated the expression levels of p16, p21 and p53, which are major upstream regulators of the G1/S cell–cycle checkpoint and cellular senescence (Fig. 7D) [29]. The above data suggested that compounds **1**, **5** and **6** induced G0/G1 arrest and senescence in L1210 cells and that p53, p21, and p16 may involve in this process. Taken together, compounds **1**, **5** and **6** inhibited proliferation, induced G0/G1 cell cycle arrest, senescence and mitochondria-mediated apoptosis in L1210 cells.

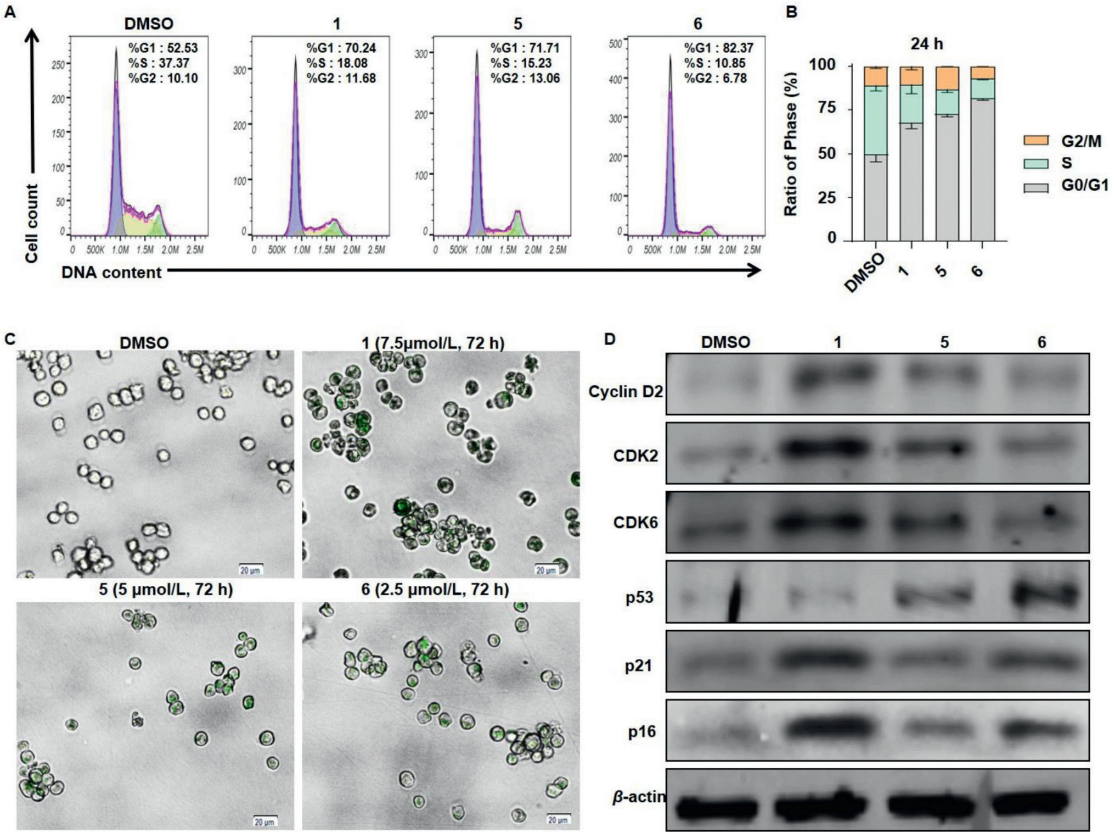

Fig. 7. Compounds **1**, **5** and **6** induced G0/G1 cell cycle arrest and senescence in L1210 cells. (A, B) Effects of compounds **1**, **5** and **6** on cell cycle progressions of L1210 cells. After treated with compounds **1** (10 μmol/L), **5** (10 μmol/L) and **6** (5 μmol/L) for 24 h, cell cycle distribution was analysed with PI staining and FACS. Columns, means of three different experiments; bars, SD, $^{**}P < 0.01$ *vs.* control group (DMSO < 0.1%). (C) Compounds **1** (7.5 μmol/L), **5** (5 μmol/L) and **6** (2.5 μmol/L) treated for 72 h induced senescence-associated β-galactosidase (SA-β-gal) activity in L1210 cells. Scale bars: 20 μm. (D) Western blot analysis of G0/G1 cell cycle and senescence related proteins after 48 h treatment. β-Actin was used as a loading control.

In conclusion, uncovered by the OSMAC and LC–MS-based molecular networking strategies, six novel phenylspirodrimane dimers and hybrids (**1–6**) were isolated and characterized from a modified large-scale culture of a coral-derived fungus *S. chartarum*. Structurally, compounds **1–6** represent a series of skeletally unprecedented dimeric phenylspirodrimanes by an unexpected linkage between C-18 and C-23′, simultaneously compounds **1–3** are uniquely defined by an unexpected 5-methyl-1,3-benzenediol moiety *via* a carbon-carbon linkage. The mechanism of action investigation revealed that compounds **1**, **5** and **6** induced cell proliferation inhibition, G0/G1 phase cell cycle arrest and senescence, leading to mitochondria-mediated apoptosis in L1210 cells. Our current findings provide two novel classes of phenylspirodrimane dimers and hybrids as promising candidate molecules for hematological leukemia treatment research.

Declaration of competing interest

The authors have no conflicts of interest to declare.

Acknowledgments

We thank the Analytical and Testing Center at Huazhong University of Science and Technology for measuring ECD, IR, UV and single-crystal X-ray diffraction data. This project was financially supported by the National Natural Science Foundation for Distinguished Young Scholars (No. 81725021), the Innovative Research Groups of the National Natural Science Foundation of China (No. 81721005), the National Natural Science Foundation of China (No. 81573316), the Fundamental Research Funds for the Central Universities (Nos. 2020kfyXJJS083, 2021yjsCXCY094 and 2172019kfyXJJS166), the Tongji-Rongcheng Center for Biomedicine, Huazhong University of Science and Technology (No. 0231514141), the Research and Development Program of Hubei Province (No. 2020BCA058), and the Hubei Provincial Natural Science Foundation of China (No. 2019CFB646).

Supplementary materials

Supplementary material associated with this article can be found, in the online version, at doi:10.1016/j.cclet.2022.03.064.

References

[1] F. Martínez-Jiménez, F. Muiños, I. Sentís, et al., Nat. Rev. Cancer 20 (2020) 555–572.
[2] J. Ferlay, M. Colombet, I. Soerjomataram, et al., Int. J. Cancer 149 (2020) 778–789.
[3] H. Sung, J. Ferlay, R.L. Siegel, et al., Ca-Cancer J. Clin. 71 (2021) 209–249.
[4] N. Li, Q. Sun, Z. Yu, et al., ACS Nano 12 (2018) 5197–5206.
[5] L. Zhao, X. Xiong, L. Liu, et al., Chin. Chem. Lett. 33 (2022) 1841–1849.
[6] Y. Tan, Z. Guo, M. Zhu, et al., Chin. Chem. Lett. 31 (2020) 1406–1409.
[7] H. Sun, H. Li, J. Wang, G. Song, Chin. Chem. Lett. 29 (2018) 977–980.
[8] B. Shen, Cell 163 (2015) 1297–1300.
[9] D.J. Newman, G.M. Cragg, J. Nat. Prod. 83 (2020) 770–803.
[10] E. Patridge, P. Gareiss, M.S. Kinch, D. Hoyer, Drug Discov. Today 21 (2016) 204–207.
[11] L. Ouyang, Y. Luo, M. Tian, et al., Cell Prolif. 47 (2014) 506–515.
[12] P.S. Rawat, A. Jaiswal, A. Khurana, J.S. Bhatti, U. Navik, Biomed. Pharmacother. 139 (2021) 111708.
[13] M. Liu, W. Sun, L. Shen, et al., Angew. Chem. Int. Ed. 58 (2019) 12091–12095.
[14] F. Li, W. Sun, J. Guan, et al., Org. Lett. 20 (2018) 7982–7986.
[15] Z. Hu, W. Sun, F. Li, et al., Org. Lett. 20 (2018) 5198–5202.

[16] F. Li, S. Lin, S. Zhang, et al., Org. Lett. 21 (2019) 8353–8357.
[17] W. Gao, C. Chai, Y. He, et al., Org. Lett. 21 (2019) 8469–8472.
[18] F. Li, W. Sun, S. Zhang, et al., Chin. Chem. Lett. 31 (2020) 197–201.
[19] B. Yang, Y. He, S. Lin, et al., J. Nat. Prod. 82 (2019) 1923–1929.
[20] J. Zhao, J. Feng, Z. Tan, et al., J. Nat. Prod. 80 (2017) 1819–1826.
[21] X.H. Ma, W.M. Zheng, K.H. Sun, et al., Nat. Prod. Res. 33 (2019) 386–392.
[22] P. Zhang, Y. Li, C. Jia, et al., RSC Adv. 7 (2017) 49910–49916.
[23] R. Kaneto, K. Dobashi, I. Kojima, et al., J. Antibiot. 47 (1994) 727–730.
[24] Z. Hu, Y. Ye, Y. Zhang, Nat. Prod. Rep. 38 (2021) 1775–1793.
[25] J. Liu, X. Jia, J. Zhao, et al., Org. Chem. Front. 7 (2020) 531–542.
[26] K. Hasumi, E. Suzuki, Int. J. Mol. Sci. 22 (2021) 954.
[27] J.I. Choi, S.H. Park, H.J. Lee, D.W. Lee, H.N. Lee, PLoS One 11 (2016) e0155052.
[28] Z. Mao, Z. Ke, V. Gorbunova, A. Seluanov, Aging 4 (2012) 431–435.
[29] Y. Kulaberoglu, R. Gundogdu, A. Hergovich, Genome Stability 15 (2016) 243–256.